Minimum Energy Trajectory Planning Method for Robot Manipulator Mounted on Flexible Base

Akira Abe
Department of Systems, Control and Information Engineering
Asahikawa National College of Technology
Asahikawa 078-8142, Japan
Email: abe@asahikawa-nct.ac.jp

***Abstract*—This paper proposes a minimum energy trajectory planning method with residual vibration reduction for a robot manipulator mounted on flexible base, in which a point-to-point motion task of the manipulator is considered. In the proposed method, the joint angle of the robot manipulator is generated by radial basis function networks (RBFNs). The maximum residual vibration amplitude and operating energy are adopted as the objective functions, and then, the RBFNs are tuned by an elitist non-dominated sorting genetic algorithm (NSGA–II). The trajectory obtained using the proposed method can suppress the residual vibration of the flexible base in energy conservation. Results obtained from simulations reveal a trade-off relationship between the residual vibration amplitude and the operating energy. Furthermore, the validity of the proposed method is confirmed experimentally.**

I. Introduction

Vibration control problems for flexible structures have great importance in many engineering applications such as space and industrial robotic systems. A considerable number of papers are therefore available on the vibration control of flexible structures. Singhose [1] presented a review of the command shaping technique, which is a well-known method for suppressing unwanted transient deflection and residual vibration of flexible systems. A review on various vibration control techniques applicable to flexible manipulators, which are basic components of industrial and space robots, was published by Benosman and Vey [2]. Dwivedy and Eberhard [3] also compiled a comprehensive list of publications (up to 2005), dealing with the dynamic analysis and control of flexible manipulators.

Regarding the studies dealing with the vibration control of a robotic manipulator mounted on a flexible base, Torres et al. [4] investigated the problem of planning manipulator motion to reduce vibration in elastically mounted space manipulator systems. To improve the performance of time-domain pre-filtering techniques, they used a coupling map for describing the dynamic interaction between a manipulator and its flexible supporting structure. A composite control law for end-effector path tracking with a flexible structure mounted manipulator system was proposed by Nenchev et al. [5], in which they revealed that base vibration suppression in a system without energy dissipation results in a change in the coupling momentum. George and Book [6] presented research on developing a control scheme to provide position control and enhanced vibration damping of a rigid manipulator attached to a flexible but unactuated base. Ott et al. [7] proposed a Cartesian compliance controller for a manipulator mounted on a flexible base that did not require any measurement of the base motion. Yang et al. [8] addressed neural network-based adaptive output feedback augmentation of an existing combined position and vibration control system for a flexible base manipulator. Fuzzy logic controllers for robot manipulators mounted on an oscillatory base were investigated by Lin et al. [9], [10], who also developed novel pseudo-inverse Jacobian feedback control laws [11]. Fukazu et al. [12] developed a method for motion control combined with vibration suppression [13] of a redundant manipulator on a flexible base, and reported that kinematic redundancy was helpful in reducing vibration in flexible-base manipulators. The present author [14] specifically examined a point-to-point (PTP) motion task of a rigid robot manipulator attached to a flexible link and presented an optimal trajectory planning technique for suppressing residual vibrations of the flexible link, in which soft computing techniques were used to construct the control scheme easily.

On the other hand, in recent years, it has been desirable to reduce the mechanical energy of robot actuators for conserving energy. However, to the best of the author's knowledge, no studies have been conducted on minimum energy trajectory planning methods with vibration reduction for flexible robotic manipulators, and studies on the topic have been confined to rigid manipulators (e.g., [15], [16], [17]). Taking this background into consideration, the present author and Komuro [18] dealt with a PTP motion task for a flexible manipulator and developed a minimum energy trajectory planning method for residual vibration suppression. In this method, an artificial neural network (ANN) was used to generate the desired joint angle and the ANN was learned by a vector-evaluated particle swarm optimization algorithm [19].

This paper reports the development of a trajectory planning method based on a multi-objective optimization approach for simultaneously suppressing the residual vibration and operating energy of a robot manipulator mounted on flexible base with a PTP motion. The robot manipulator has one revolution joint. In the proposed method, we attempt to generate the trajectory of the joint angle by using radial basis function networks (RBFNs) such as that described in an earlier report [20]. To obtain the desired trajectory, the RBFNs are tuned by

978-1-4673-5769-2/13/$31.00 ©2013 IEEE

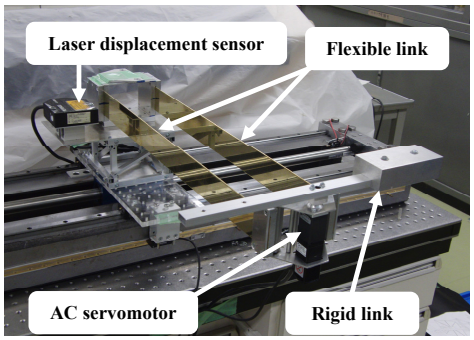

Fig. 1. Photograph of experimental setup.

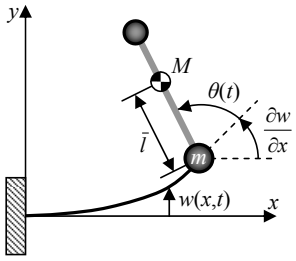

Fig. 2. Mathematical model of experimental setup.

an elitist non-dominated sorting genetic algorithm (NSGA–II) [21], which is a multi-objective optimization algorithm. When the robot manipulator is operated along the obtained trajectory, the residual vibration suppression of the flexible base can be realized with minimum driving energy consumption. In other words, the proposed method is an open-loop control that does not require sensors to measure unwanted vibrations. Simulation and experimental results demonstrate the effectiveness of the proposed vibration control scheme for the suppression of residual vibrations. Furthermore, the effect of not only the vibration suppression but also the energy conservation is also confirmed.

II. Experimental Setup

An overview and mathematical model of the experimental setup used in the present study are shown respectively in Figs. 1 and 2. As shown in Fig. 1, we employ an elastic parallel beam, which is made of a brass beam of length l, width b, and thickness h, as the flexible base. The flexible link is clamped at one end. The other end is free to vibrate. The displacement w of the flexible link is measured using a laser displacement sensor (LK-035; Keyence Co.), which is placed at a distance of 50 mm from the clamped end. An AC servomotor (SGMMJ; Yaskawa Electric Corp.) is used to drive the rigid link, whose mass is M and center of gravity is $\bar{l}$. The joint angle θ of the rigid link is measured by a serial encoder mounted on the servomotor. The servomotor is operated in the speed control mode using a servo drive (SGDS; Yaskawa Electric Corp.). The motor torque τ is monitored using the servo drive. Table I lists the parameters of the experimental setup, in which m is the tip mass including the mass of the servomotor.

TABLE I
Parameters of Experimental Setup

Parameter	Value	Unit
l	550	[mm]
b	50	[mm]
h	1.6	[mm]
M	450	[g]
$\bar{l}$	105	[mm]
m	635	[g]

To achieve tracking control of the joint angle in the experimental setup, the following control law, which consists of PD control and feedforward control, is used.

$$v = K_1(\theta_{ref} - \theta) + K_2(\dot{\theta}_{ref} - \dot{\theta}) + v_{ref}. \tag{1}$$

Here, v denotes the input voltage supplied to the servo drive in the speed control mode, and θ_{ref} and $\dot{\theta}_{ref}$ respectively denote the given reference angle and velocity. The variable v_{ref} is the reference voltage corresponding to $\dot{\theta}_{ref}$ in the speed control mode. The feedback gains of the PD control are denoted by K_1 and K_2, which are set to 20 and 0.1, respectively. Measurement and control of the experimental setup are implemented on a DSP board (DS1104; dSPACE GmbH), with a sampling time of 2 ms.

III. Mathematical Model

In this section, we derive the equations of motion for the robotic manipulator attached to a flexible link, as sketched in Fig. 2. The values of the parameters in the equations of motion are determined from an identification experiment.

A. Equations of Motion

The position vector $\boldsymbol{r}$ of the center of mass of the rigid link can be expressed as

$$\boldsymbol{r} = \begin{bmatrix} r_x \\ r_y \end{bmatrix} = \begin{bmatrix} l + \bar{l}\cos\{\theta + w'(l,t)\} \\ w(l,t) + \bar{l}\sin\{\theta + + w'(l,t)\} \end{bmatrix}, \tag{2}$$

where a prime denotes the partial derivative with respect to x. The kinetic energy $\mathscr{T}$ of the system can be written as

$$\mathscr{T} = \frac{1}{2}\left[\rho\int_0^l \dot{w}(x,t)^2 dx + m\dot{w}(l,t)^2 + M\dot{\boldsymbol{r}}^{\mathrm{T}}\dot{\boldsymbol{r}}\right], \tag{3}$$

where ρ is the mass per length of the flexible link. We assume that the flexible link is an Euler-Bernoulli beam, and then obtain the potential energy $\mathscr{U}$ of the system as follows:

$$\mathscr{U} = \frac{EI}{2}\int_0^l \left[w''(x,t)\right]^2 dx. \tag{4}$$

With regard to the dynamic behavior of the flexible link, we assume that the first vibration mode is the dominant mode during the PTP motion of the rigid link, with higher modes being of significantly small amplitudes. Therefore, the displacement w of the flexible link is approximated by the

eigenfunction $\phi(x)$ of the first vibration mode for a cantilever beam with a tip mass:

$$w(x,t) = \phi(x)W(t), \tag{5}$$

where $W(t)$ is a time function. The equations of motion for the system can be obtained from the Lagrangian approach, which is represented as follows:

$$\frac{d}{dt}\left(\frac{\partial \mathscr{L}}{\partial \dot{W}}\right) - \frac{\partial \mathscr{L}}{\partial W} = 0, \quad \frac{d}{dt}\left(\frac{\partial \mathscr{L}}{\partial \dot{\theta}}\right) - \frac{\partial \mathscr{L}}{\partial \theta} = \tau, \tag{6}$$

where $\mathscr{L} = \mathscr{T} - \mathscr{U}$. By substituting (3) and (4) into (6) and using (2) and (5), the nonlinear equations in terms of the flexible and rigid links can be derived respectively as

$$\begin{aligned}&[1 + \alpha_1 \cos(\theta + \gamma W)]\ddot{W} + 2\zeta\omega\dot{W} + \omega^2 W \\ &\quad + [\alpha_2 + \alpha_3 \cos(\theta + \gamma W)]\ddot{\theta} \\ &\quad + \left(\alpha_4 \dot{W}\dot{\theta} - \alpha_3 \dot{\theta}^2 + \alpha_5 \dot{W}^2\right)\sin(\theta + \gamma W) = 0, \end{aligned} \tag{7}$$

$$\beta_1 \ddot{\theta} + c\dot{\theta} + [\beta_2 + \beta_3 \cos(\theta + \gamma W)]\ddot{W} = \tau, \tag{8}$$

where ζ and c respectively represent the viscous damping and friction coefficients, which are introduced because of the experimental setup.

B. Identified Parameters

The performance of open-loop controllers is well known to be dependent on the accuracy of the mathematical models of controlled objects. Therefore, precision mathematical models must be used. Consequently, to obtain the mathematical model of the system accurately, we perform an identification experiment and then determine the values of the coefficients in (7) and (8).

The parameter identification technique [22] is described below. First of all, the joint angle is rotated along a cycloidal motion

$$\theta_{cyc}(t) = \Delta\theta\left[\frac{t}{T_E} - \frac{1}{2\pi}\sin\left(\frac{2\pi t}{T_E}\right)\right] + \theta_S, \quad (0 \le t \le T_E), \tag{9}$$

where, $\Delta\theta = \theta_E - \theta_S$, and θ_S and θ_E respectively denote initial and final joint angles. The traveling time is indicated by T_E. Then, the displacements of the flexible link and the driving torque of the AC servomotor are measured. Next, the values of the coefficients in (7) and (8) are sought so that the displacement and torque obtained by numerical simulation coincide with the experimentally obtained results. This parameter tuning is performed by using a particle swarm optimization technique [23]; then, the accurate mathematical model can be obtained. The identified results are presented in Table II. It is noteworthy that the parameters α_5 and γ are negligible (i.e., the values are equal to zero) because their effect on the dynamics is very small.

Fig. 3 shows a comparison of time histories obtained by the simulation and experiment, in the case when the joint angle is rotated along the cycloidal motion. The driving condition is set as ($T_E = 1.0$ s, $\theta_S = -\pi/2$ rad, and $\theta_E = \pi/4$ rad). Figs. 3(a)–3(d) respectively depict the joint angle, angular velocity, tip displacement, and motor torque. In Figs. 3(a) and 3(b), the solid and dotted lines respectively indicate the experimental results and the reference values, which are in perfect agreement with each other. Thus, it can be inferred that the tracking control based on (1) is valid. In addition, as portrayed in Figs. 3(c) and 3(d), the experimental results (represented by the solid line) are in good agreement with the simulation results (represented by the dotted line). Therefore, we can confirm that the parameter identification is accurate. On the other hand, from Fig. 3(c), we observe that residual vibrations (i.e., the displacement after positioning) occur in this case. The next section presents a trajectory planning method for canceling the residual vibrations with minimum driving energy consumption.

TABLE II
IDENTIFIED PARAMETERS

Parameter	Value	Unit
α_1	-0.1055	[–]
α_2	-9.949×10^{-3}	[m]
α_3	5.256×10^{-2}	[m]
α_4	7.634×10^{-2}	[–]
ζ	1.500×10^{-3}	[–]
β_1	5.366×10^{-3}	[kgm^2]
β_2	-4.944×10^{-3}	[kgm]
β_3	2.399×10^{-2}	[kgm]
c	1.965×10^{-2}	[Nms]
ω	7.320	[rad/s]

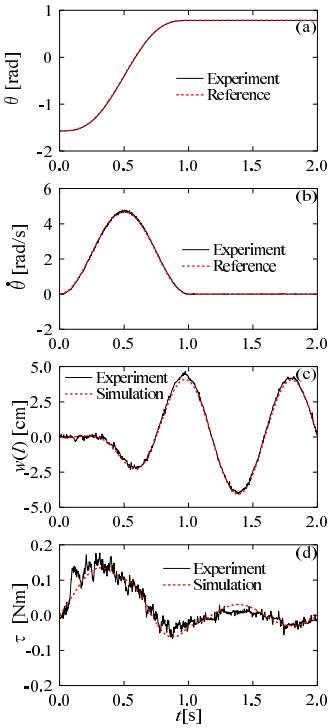

Fig. 3. Comparison of simulation and experimental results obtained by the cycloidal motion ($T_E = 1.0$ s, $\theta_S = -\pi/2$ rad, and $\theta_E = \pi/4$ rad): (a) joint angle, (b) angular velocity, (c) tip displacement, and (d) motor torque.

IV. Minimum Energy Trajectory Planning Method

The present study focuses on a PTP motion of the rigid manipulator attached to the flexible link when the joint angle is rotated from an initial angle θ_S to a target angle θ_E in a travelling time T_E. In order to simultaneously minimize the residual vibration and operating energy, we develop the optimal trajectory planning method for the joint angle.

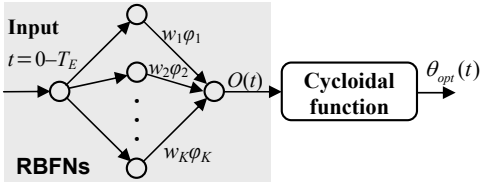

Fig. 4. Schematic diagram of trajectory generation.

A schematic diagram of the trajectory generation adopted here is illustrated in Fig. 4. As Fig. 4 shows, we employ RBFNs, which consist of an input layer, K neurons in the hidden layer, and an output layer, to generate the optimal trajectory [20]. The input of the RBFNs is given by time t until the travelling time T_E. The output of the kth hidden layer is expressed as follows using a Gaussian function:

$$\varphi_k(t) = \exp\left[-\frac{(t-c_k)^2}{\sigma_k^2}\right], \quad (k = 1,2,\cdots,K). \tag{10}$$

Here, c_k is the center of the basis function and σ_k is the variance representing the spread of the basis function. The output of the RBFNs is given as

$$O(t) = \sum_{k=1}^{K} w_k \varphi_k(t), \tag{11}$$

where w_k is the weight between the hidden and output layers. Finally, by providing the output of the RBFNs to the input of the cycloidal function

$$\Phi(u) = \Delta\theta\left[u - \frac{\sin(2\pi u)}{2\pi}\right] + \theta_S, \tag{12}$$

the trajectory of the joint angle is generated as

$$\theta_{opt}(t) = \Phi[O(t)]. \tag{13}$$

The trajectory naturally satisfies the boundary conditions as

$$\theta_{opt}(0) = \theta_S, \quad \theta_{opt}(T_E) = \theta_E. \tag{14}$$

By considering (12), the conditions in (14) can be rewritten as

$$O(0) = 0, \quad O(T_E) = 1. \tag{15}$$

To satisfy the above conditions, the weights w_{K-1} and w_K are determined from the following equations:

$$\left.\begin{aligned} &\sum_{k=1}^{K-2} w_k\varphi_k(0) + w_{K-1}\varphi_{K-1}(0) + w_K\varphi_K(0) = 0 \\ &\sum_{k=1}^{K-2} w_k\varphi_k(T_E) + w_{K-1}\varphi_{K-1}(T_E) + w_K\varphi_K(T_E) = 1 \end{aligned}\right\}. \tag{16}$$

Moreover, differentiating (13) with respect to time leads to the profiles of the angular velocity and acceleration:

$$\dot{\theta}_{opt}(t) = 2\Delta\theta\sin^2[\pi O(t)]\dot{O}(t), \tag{17}$$

$$\begin{aligned}\ddot{\theta}_{opt}(t) &= 2\Delta\theta\sin[\pi O(t)] \\ &\times\left\{2\pi\cos[\pi O(t)]\dot{O}^2(t) + \sin[\pi O(t)]\ddot{O}(t)\right\}. \end{aligned}\tag{18}$$

From the conditions in (15), we can confirm that the angular velocity and acceleration satisfy the following boundary conditions:

$$\dot{\theta}_{opt}(0) = \dot{\theta}_{opt}(T_E) = \ddot{\theta}_{opt}(0) = \ddot{\theta}_{opt}(T_E) = 0. \tag{19}$$

Therefore, the procedure described above generates smooth motion, because of which not only the angular velocity but also acceleration is equal to zero at the start and end points in the PTP motion.

The trajectory of the joint angle generated by (13) is a function of parameters c_k, σ_k, and w_k of the RBFNs. Consequently, we tune the parameters to simultaneously minimize the residual vibration and operating energy. For this purpose, we define the following two objective functions

$$F_1 = |W_{\max}|, \quad F_2 = \int_0^{\Delta\theta} |\tau| d\theta, \tag{20}$$

where $|W_{\max}|$ denotes the maximum tip displacement of the flexible link in 1 s after the positioning of the rigid link. It is noteworthy that F_2 represents the operating energy of the joint angle until positioning. In the present study, NSGA–II [21] is applied to simultaneously minimize the two objective functions.

The algorithm for the trajectory planning method based on the NSGA–II algorithm is summarized as follows. First of all, we designate a driving condition (T_E, θ_S, and θ_E). Using the trajectory obtained from (13), (17), and (18), the displacement of the flexible link is calculated by numerically integrating (7). The inverse dynamics analysis of (8) yields the driving torque τ. The two objective functions are then obtainable. The two objective functions are minimized using NSGA–II, in which the parameters $c_1, c_2, \cdots, c_K$, $\sigma_1, \sigma_2, \cdots, \sigma_K$, and $w_1, w_2, \cdots, w_{K-2}$ are considered to be optimized. By rotating the rigid link along the trajectory obtained using this algorithm, residual vibrations of the flexible link can be suppressed in energy conservation; that is, an energy-conserving open-loop controller can be established.

V. Results and Discussion

To verify the validity of the energy-conserving open-loop control technique described in the previous section, we present some results obtained from simulations and experiments. In the following results, the number of hidden layers in the RBFNs is set to $K = 6$. In the NSGA–II algorithm, the number of populations, total number of generations, crossover rate, and mutation rate are set respectively to 200, 500, 0.8, and 0.01.

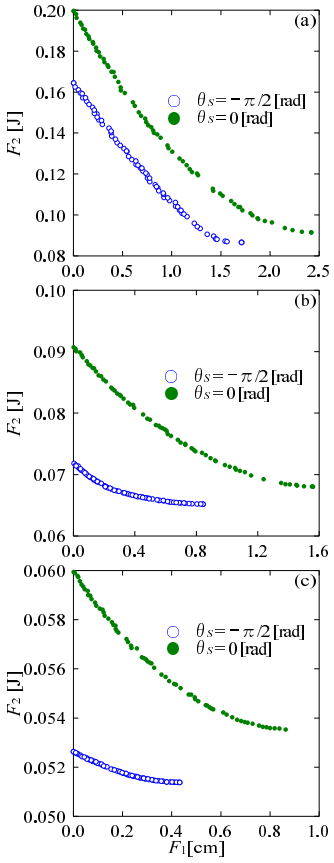

Fig. 5. Pareto optimal solutions ($\Delta\theta = \pi/2$ rad, and $\theta_S = -\pi/2$ and 0 rad): (a) $T_E = 0.8$ s, (b) $T_E = 1.0$ s, and (c) $T_E = 1.2$ s.

The search space of the tuning parameters is taken as

$$\left.\begin{aligned} c_k &\in [-5,5], \quad (k = 1,2,\cdots,K) \\ \sigma_k &\in [1,10], \quad (k = 1,2,\cdots,K) \\ w_k &\in [-100,100], \quad (k = 1,2,\cdots,K-2) \end{aligned}\right\}. \tag{21}$$

Fig. 5 shows the calculated Pareto optimal solutions for the PTP motion under the driving condition ($\Delta\theta = \theta_E - \theta_S = \pi/2$ rad), in which the symbols ○ and ● respectively indicate plots of $\theta_S = -\pi/2$ and 0 rad. The results for $T_E = 0.8$, 1.0, and 1.2 s are respectively presented in Figs. 5(a)–5(c). The abscissa F_1 represents the maximum residual vibration amplitude of the flexible link, and the ordinate F_2 represents the operating energy of the rigid link. As Fig. 5 shows, the operating energy increases with a decrease in the residual vibration amplitude, and hence, a trade-off relationship exists between the two objective functions defined in (20). From the trade-off relationship, we can infer that it is necessary to add energy for suppressing residual vibrations. Moreover, in spite of the same rotation angle ($\Delta\theta = \pi/2$ rad), the distribution of the Pareto front differs strongly depending on the initial angle θ_S. Therefore, we can say that the optimal trajectory for the rigid link is strongly dependent on the initial angle.

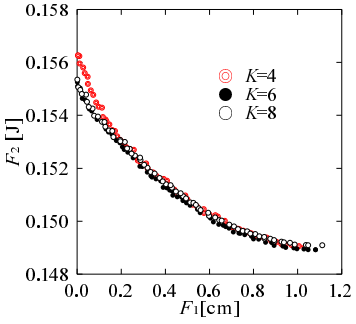

Fig. 6. Effect of the number of hidden layers on the Pareto optimal solutions ($T_E = 1.0$ s, $\theta_S = -\pi/2$ rad, $\theta_E = \pi/4$ rad).

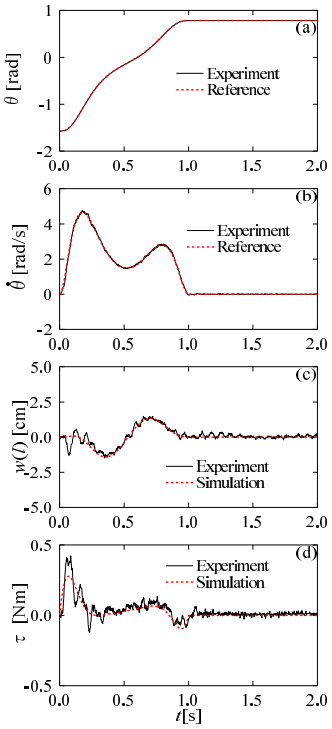

Fig. 7. Comparison of simulation and experimental results obtained by the proposed method ($T_E = 1.0$ s, $\theta_S = -\pi/2$ rad, and $\theta_E = \pi/4$ rad): (a) joint angle, (b) angular velocity, (c) tip displacement, and (d) motor torque.

Fig. 6 shows the effect of the number of hidden layers in the RBFNs on the Pareto optimal solutions, in which the driving condition is set as ($T_E = 1.0$ s, $\theta_S = -\pi/2$ rad, and $\theta_E = \pi/4$ rad). As can be seen in Fig. 6, there is no large difference in the Pareto optimal set even when the number of hidden layers increases. However, F_1 becomes smaller than 0.1 cm, the results for $K = 4$ deviate from those for $K = 6$ and 8; that is, the operating energy obtained from $K = 4$ is larger than those obtained from $K = 6$ and 8. Therefore, to suppress not only the residual vibration but also operating energy, the number of hidden layers must be equal to or larger than 6.

To demonstrate the feasibility of the proposed method for residual vibration suppression with minimum driving energy consumption, we carry out the following experiment. Here-

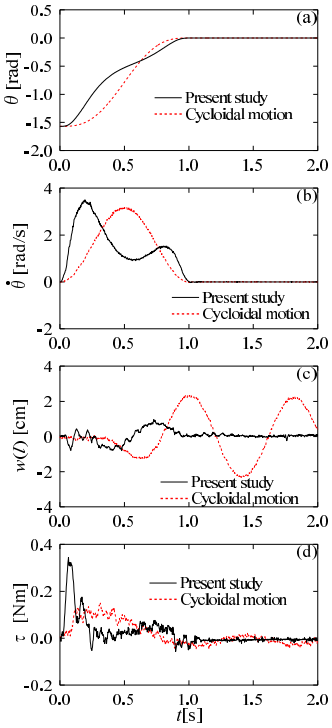

Fig. 8. Comparison of experimental results obtained by the proposed method and cycloidal motion ($T_E = 1.0$ s, $\theta_S = -\pi/2$ rad, and $\theta_E = 0$): (a) joint angle, (b) angular velocity, (c) tip displacement, and (d) motor torque.

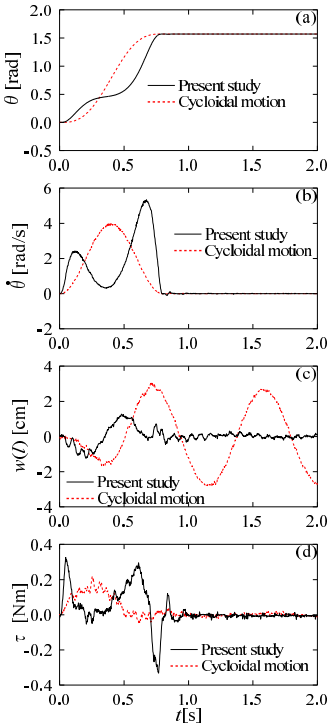

Fig. 9. Comparison of experimental results obtained by the proposed method and cycloidal motion ($T_E = 0.8$ s, $\theta_S = 0$, and $\theta_E = \pi/2$ rad): (a) joint angle, (b) angular velocity, (c) tip displacement, and (d) motor torque.

after, the best solution for residual vibration suppression in the Pareto set is referred to as the optimal trajectory. Fig. 7 shows a comparison of the simulation and experimental results when the rigid link is driven along the optimal trajectory under the same conditions as those shown in Fig. 3. It can be observed from Figs. 7(a) and 7(b) that the experimental results agree perfectly with the reference values, and hence, we can reconfirm the validity of the tracking control of the rigid link, which is explained in Section II. As portrayed in Fig. 7(c), the influence of higher vibration modes can be observed in the time region from zero to about 0.25 s. As can be seen in Fig. 7(d), torque fluctuation occurs in the time region because of the influence. On the other hand, residual vibrations occur in the case of the cycloidal motion (see Fig. 3(c)), whereas they are sufficiently suppressed in the proposed method (see Fig. 7(c)). Moreover, the simulation and experimental results for the tip displacement and motor torque are in reasonable agreement with each other. Therefore, it can be said that the mathematical modeling and trajectory planning method developed in this study are valid and effective.

In order to further check the validity of the proposed method for suppressing the residual vibration, we change the driving conditions and then perform the simulations and experiments. A comparison of the experimental results obtained for the optimal trajectory (solid line) and cycloidal motion (dotted line) is presented in Figs. 8 and 9. Figs. 8 and 9 respectively show the results under the driving conditions ($T_E = 1.0$ s, $\theta_S = -\pi/2$ rad, and $\theta_E = 0$) and ($T_E = 0.8$ s, $\theta_S = 0$, and $\theta_E = \pi/2$ rad). It is found from Figs. 8(c) and 9(c) that residual vibrations occur in the case of the cycloidal motion. As depicted in Fig. 9(c), the flexible link vibrates slightly after positioning when the manipulator is driven along the optimal trajectory, owing to the influence of the higher vibration modes. However, compared to the cycloidal motion, the proposed method has superior performance for the residual vibration suppression. Furthermore, devoting attention to the displacements when the rigid link is rotating, it can be seen in Figs. 3(c), 7(c), 8(c), and 9(c) that the maximum amplitudes obtained by the proposed method are smaller than those obtained by the method in which the cycloidal motion is used. Hence, we can say that the proposed method also has the capability of reducing the vibration during a PTP motion.

Finally, we mention the effect of energy conservation in the

TABLE III
COMPARISON OF OPERATING ENERGY F_2 [J]

Figure	Proposed method	Cycloidal motion
3, 7	0.206	0.212
	(0.155)	(0.209)
8	0.103	0.111
	(7.18×10^{-2})	(8.72×10^{-2})
9	0.235	0.145
	(0.200)	(0.125)

proposed method. From the graphs presented above, we can prove that the proposed method minimizes the objective function F_1 in (20). However, we cannot evaluate the minimization of the operating energy F_2 using the proposed method. Thus, we list the operating energy of the servomotor obtained from the experiments in Table III. The values in parentheses denote the simulation results. It can be observed from Table III that the values of the experimental results are larger than those of the simulation results. This fact is attributed to the influences of the higher vibration modes and motor frictions that are not considered in the modeling. On the other hand, under the driving conditions used to obtain the results shown in Figs. 7 and 8, the values for the optimal trajectory are smaller than those for the cycloidal motion inducing large residual vibrations. Thus, we can reconfirm the superiority of the proposed method. However, the proposed method cannot reduce the operating energy in comparison to the cycloid motion under the driving conditions used to obtain the results shown in Fig. 9. As also shown in Fig. 5, this implies that the operating energy for residual vibration suppression depends on the driving condition, especially the initial angle.

VI. Summary

In the present study, we dealt with a PTP motion task of a robotic manipulator attached to a flexible link, and developed an optimal trajectory planning method, which was based on a multi-objective optimization technique, for simultaneously suppressing the residual vibration of the flexible link and the operating energy of the manipulator. For this purpose, the maximum amplitude of the residual vibration and the operating energy of the manipulator until positioning were defined as the objective functions. RBFNs were utilized to generate the desired trajectory. By using the NSGA–II algorithm, the parameters of the RBFNs were tuned to minimize the two objective functions, and then, the optimal trajectory could be obtained. From simulation results, we revealed that a trade-off relationship existed between the residual vibration amplitude and the operating energy. To demonstrate the feasibility of the proposed method, we also performed experiments. The experimental results demonstrated that the proposed method is effective for residual vibration suppression. Moreover, we showed that under some driving conditions, the operating energy for the optimal trajectory suppressing residual vibrations was lower than that for the cycloidal motion inducing large residual vibrations. Therefore, by using the proposed method, the residual vibrations could be suppressed under the minimum energy condition.

Acknowledgment

The author wishes to thank Mr. Hiroki Tanno, a student at Asahikawa National College of Technology, for his assistance in improving the experimental setup.

References

[1] W. Singhose, "Command shaping for flexible systems: A review of the first 50 years," *International Journal of Precision Engineering and Manufacturing*, vol. 10, no. 4, pp. 153–168, 2009.

[2] M. Benosman and L. G. Vey, "Control of flexible manipulators: A survey," *Robotica*, vol. 22, no. 5, pp. 535–545, 2004.

[3] S. K. Dwivedy and P. Eberhard, "Dynamic analysis of flexible manipulators, A literature review," *Mechanism and Machine Theory*, vol. 41, no. 7, pp. 749–777, 2006.

[4] M. A. Torres, S. Dudowsky and A. C. Pisoni, "Path-planning for elastically-mounted space manipulators: Experimental evaluation of the Coupling Map," in *Proc. IEEE Int. Conf. Robotics and Automation*, San Diego, CA, 1994, pp. 2227–2233.

[5] D. N. Nenchev, K. Yoshida, P. Vichitkulsawat and M. Uchiyama, "Reaction null-space control of flexible structure mounted manipulator systems," *IEEE Trans. Robotics and Automation*, vol. 15, no. 1, pp. 1011–1023, 1999.

[6] L. E. George and W. J. Book, "Inertial vibration damping of a flexible base manipulator," *JSME International Journal Series C*, vol. 46, no. 3, pp. 789–806, 2003.

[7] C. Ott, A. Albu-Schaffer and G. Hirzinger, "A Cartesian compliance controller for a manipulator mounted on a flexible structure," in *Proc. IEEE/RSJ Int. Conf. Intelligent Robots and Systems*, Beijing, China, 2006, pp. 4502–4508.

[8] B. J. Yang, A. J. Calise and J. I. Craig, "Adaptive output feedback control of a flexible base manipulator," *Journal of Guidance, Control, and Dynamics*, vol. 30, no. 4, pp. 1068–1080, 2007.

[9] J. Lin and Z. Z. Huang, "A hierarchical fuzzy approach to supervisory control of robot manipulators with oscillatory bases," *Mechatronics*, vol. 17, no. 10, pp. 589–600, 2007.

[10] J. Lin, Z. Z. Huang and P. H. Huang, "An active damping control of robot manipulators with oscillatory bases by singular perturbation approach," *Journal of Sound and Vibration*, vol. 304, no. 1–2, pp. 345–360, 2007.

[11] J. Lin, C. C. Lin and H. S. Lo, "Pseudo-inverse Jacobian control with grey relational analysis for robot manipulators mounted on oscillatory bases," *Journal of Sound and Vibration*, vol. 326, no. 3–5, pp. 421–437, 2009.

[12] Y. Fukazu, N. Hara, T. Hishinuma, D. Sato and Y. Kanamiya, "Pseudoinverse-based motion control of a redundant manipulator on a flexible base with vibration suppression," *Journal of Robotics and Mechatronics*, vol. 20, no. 4, pp. 621–627, 2008.

[13] T. Hishinuma and D. N. Nenchev, "Singularity-consistent vibration suppression control with a redundant manipulator mounted on a flexible base," in *Proc. IEEE/RSJ Int. Conf. Intelligent Robots and Systems*, Beijing, China, 2006, pp. 3237–3242.

[14] A. Abe, "Residual vibration suppression for robot manipulator attached to a flexible link by using soft computing techniques," in *Proc. IEEE Int. Conf. Robotics and Biomimetics*, Phuket, Thailand, 2011, pp. 4502–4508.

[15] E. J. S. Pires, P. B. M. Oliveira and J. A. T. Machado, "Manipulator trajectory planning using a MOEA," *Applied Soft Computing*, vol. 7, no. 3, pp. 659–667, 2007.

[16] R. Saravanan and S. Ramabalan, "Evolutionary minimum cost trajectory planning for industrial robots," *Journal of Intelligent and Robotic Systems*, vol. 52, no. 1, pp. 45–77, 2008.

[17] A. Gasparetto, P. Boscariol, A. Lanzutti and R. Vidoni, "Trajectory planning in robotics," *Mathematics in Computer Science*, vol. 6, no. 3, pp. 269–279, 2012.

[18] A. Abe and K. Komuro, "Minimum energy trajectory planning for vibration control of a flexible manipulator using a multi-objective optimisation approach," *International Journal of Mechatronics and Automation*, vol. 2, no. 4, pp. 286–294, 2012.

[19] K. E. Parsopoulos, D. E. Tasoulis and M. N. Vrahatis, "Multi-objective optimization using parallel vector evaluated particle swarm optimization," in *Proc. IASTED Int. Conf. Artificial Intelligence and Applications*, Innsbruck, Austria, 2004, vol. 2, pp. 823–828.

[20] A. Abe, "Anti-sway control for overhead cranes using neural networks," *Journal of Innovative Computing, Information and Control*, vol. 7, no. 7(B), pp. 4251–4262, 2011.

[21] K. Deb, A. Pratap, S. Agarwal and T. Meyarivan, "A fast and elitist multi-objective genetic algorithm: NSGA–II," *IEEE Transactions on Evolutionary Computation*, vol. 6, no. 2, pp. 182–197, 2002.

[22] A. Abe, "Trajectory planning for flexible Cartesian robot manipulator by using artificial neural network: Numerical simulation and experimental verification," *Robotica*, vol. 29, no. 5, pp. 797–804, 2011.

[23] M. Clerc and J. Kennedy, "The particle swarm-explosion, stability, and convergence in a multidimensional complex space," *IEEE Trans. Evolutionary Computation*, vol. 6, no. 1, pp. 58–73, 2002.